

Vibronic and Environmental Effects in Simulations of Optical Spectroscopy

Tim J. Zuehlsdorff,¹ Sapana V. Shedge,²
Shao-Yu Lu,² Hanbo Hong,² Vincent P.
Aguirre,² Liang Shi,² and Christine M. Isborn²

¹Department of Chemistry, Oregon State University, Corvallis, Oregon 97331, USA

²Chemistry and Chemical Biology, University of California Merced, Merced, California 95343, USA; email: cisborn@ucmerced.edu

Annu. Rev. Phys. Chem. YYYY. AA:1–25

[https://doi.org/10.1146/\(\(please add article doi\)\)](https://doi.org/10.1146/((please add article doi)))

Copyright © YYYY by Annual Reviews.
All rights reserved

Keywords

Franck-Condon, Ensemble, Cumulant, Nonlinear Spectroscopy, 2DES

Abstract

Including both environmental and vibronic effects is important for accurate simulation of optical spectra but remains computationally challenging. We outline two approaches that consider both the explicit atomistic environment and the vibronic transitions. Both phenomena are responsible for spectral shapes in linear spectroscopy and the electronic evolution measured in nonlinear spectroscopy. The first approach utilizes snapshots of chromophore-environment configurations for which chromophore normal modes are determined. We outline various approximations for this static approach that assumes harmonic potentials and ignores dynamic system-environment coupling. The second approach obtains excitation energies for a series of time-correlated snapshots. This dynamic approach relies on the accurate truncation of the cumulant expansion but treats the dynamics of the chromophore and the environment on equal footing. Both approaches show significant potential for making strides towards more accurate optical spectroscopy simulations of complex condensed phase systems.

1. Introduction

Improvements in theory, hardware, and data science over the last decade have enabled new capabilities in simulating the electronic spectroscopy of large molecules and condensed phase environments. These improvements include electronic structure theory and software for large-scale systems that can account for the environment at the same level of theory as the chromophore in excited state calculations,(1–4) improved polarizable embedding algorithms (5–12), the availability of high-performance computing CPU and GPU clusters that provide the ability to compute tens of thousands of calculations in a relatively short turnaround time, and new machine learning techniques that accurately predict molecular energetics(13–17). Here we focus on how these improvements enable new capabilities in combining vibronic and environmental effects for more accurate simulations of optical spectroscopy.

Both vibronic and environmental effects contribute to spectral lineshapes and energies, as well as to excited state relaxation(18–26). For a linear absorption optical spectrum, vibronic transitions beyond the 0-0 transition lead to asymmetry and often a high energy tail,(27–31) whereas environment effects lead to inhomogeneous broadening and shifts in energies(28, 30, 32? –38). For nonlinear optical spectra (e.g. two-dimensional electronic spectroscopy or transient absorption), vibronic coherences and spectral diffusion manifest through peaks shifting in energy and intensity over time as the excited state evolves.(39–50)

Vibronic effects are most often accounted for within a harmonic oscillator model for both the ground and excited states. This harmonic model requires a geometry optimization to compute the normal modes of the system. Within this model, it is straightforward to compute the vibronic transitions within the Condon approximation, generating a Franck-Condon linear absorption spectrum (51–57) (with Herzberg-Teller (18, 58–62) contributions included if state mixings should be considered). Franck-Condon spectral calculations within a harmonic model are included in many electronic structure packages, and recent advances in time-dependent Franck-Condon calculations providing an efficient route for incorporating temperature dependence that leads to population of ground state vibrational levels(22, 63, 64).

However, such harmonic model calculations traditionally do not include environmental effects in a rigorous way. Instead, because geometry optimizations and normal modes must be well-defined, often an implicit polarizable continuum model (65–69) is used for the environment. Although implicit models of the environment account for average polarization effects, important specific environmental effects are missing, such as atomistic electronic polarization and hydrogen bonding, which can lead to differences in spectral shifts and shapes(70, 71). To highlight the difference for implicit and explicit models of the environment, we show in **Figure 1** results for the Nile Red chromophore in water comparing an implicit solvent model to that obtained with explicit solvent averaged over 45 molecular dynamics (MD) configurations where the solvent environment is kept frozen and only the chromophore is optimized. In the Franck-Condon spectra in **Figure 1a**, the 0-0 vibronic transitions are energetically aligned and we see that the implicit solvent spectrum has higher intensities for the higher energy vibronic peaks. This result is consistent with the results from the spectral density calculations in **Figure 1b** that depict how various vibrational modes couple to the optical excitation. Although a couple of weak peaks are less intense in the implicit solvent spectral density, the dominant difference is that that stronger peaks corresponding to the C-C and C-N stretch frequencies of the chromophore are more intense, showing that these vibrations couple more strongly to the excitation in the implicit solvent model. The explicit solvent environment reduces the contribution of these modes, lead-

MD: Molecular dynamics, used to sample an ensemble or to obtain a time series of correlated snapshots of nuclear configurations

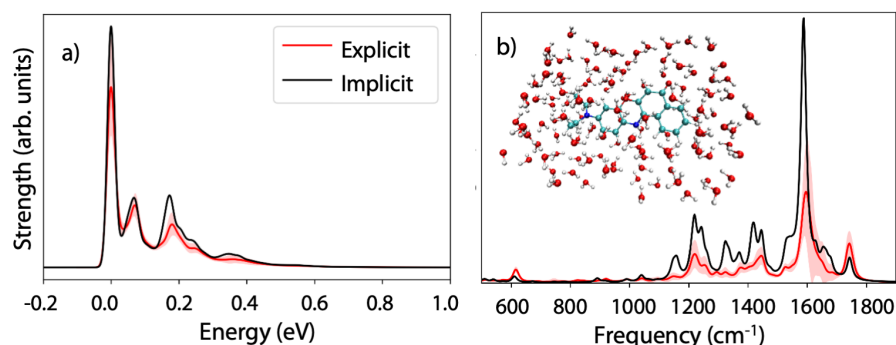


Figure 1

Explicit and implicit solvent models for the Nile red chromophore in the water. The explicit solvent results are averaged over 45 MD snapshots where the chromophore has been optimized in a frozen explicit quantum mechanical solvent environment; the pink shaded area indicates the standard deviation. (a) Zero-temperature Franck-Condon spectra, where the explicit solvent spectra are energetically aligned, shows that the implicit solvent model puts more weight on higher energy vibronic transitions compared to explicit solvent. (b) The spectral density shows that the intensity of the vibrational coupling to the electronic state is increased with implicit solvent. The inset shows the region that was treated quantum mechanically.

ing to less weight in the higher energy tail of the Franck-Condon spectrum. Interestingly, we have found that optimizing the geometry of a chromophore in the presence of explicit solvent increases the validity of the Franck-Condon principle, which we think is likely due increased overlap of the ground and excited state vibrational wave function when there is less space for the chromophore to move in the frozen environment. In some systems in implicit solvent or vacuum, the chromophore significantly changes geometry going from the ground to the excited state, resulting in negligible overlap of vibrational wave functions and no Franck-Condon spectrum. The Franck-Condon principle is built on the idea of a vertical electronic transition during which the chromophore and the environment should not undergo extensive nuclear rearrangement, meaning that large changes in geometry occurring between optimized ground and excited states should not occur on the timescale of an optical transition (51, 52, 72). The explicit solvent environment therefore provides an appealing way to generate a Franck-Condon spectrum for systems that change geometry too much within an implicit solvent model. Overall, these results show that, even for a fairly localized molecular excitation, the vibronic transitions are sensitive to the surroundings and ideally should not be considered in isolation from the atomistic environment.

Atomistic environmental effects in simulations of optical spectroscopy are commonly captured by sampling the chromophore interacting with the environment through an MD trajectory and then using many statistically independent configurations (\sim hundreds) for computing electronic excited states (1, 2, 73–81). The environment can be treated in a variety of ways during the excited state calculation, most commonly as fixed classical point charges or as a fully polarizable quantum mechanical atoms, with the classical and quantum treatment showing significant differences in excitation energy (2, 12, 38, 74, 77, 82–92). An ensemble linear absorption spectrum can be created by convoluting each of these excited state energies and oscillator strengths with a Gaussian function and summing the result. Long time scales for the MD can be achieved with classical treatment of electrons and nuclei

spectral density:

Function describing the frequency dependent coupling strength of nuclear motion to the electronic excitation

Linear and nonlinear optical spectroscopy

In linear optical spectroscopy, the response of the system is linearly proportional to the incident electric field and we consider single photon processes, including standard absorption and fluorescence spectroscopy. In nonlinear optical spectroscopy, of which there are many varieties including pump-probe, transient absorption, and two-dimensional electronic spectroscopy, the response of the system is not linearly proportional to the incident field and lasers allow us to monitor ultrafast electronic and vibronic phenomena. These processes triggered by light in the optical region of the electromagnetic spectrum correspond to transitions between the electronic ground and excited states.

using force fields, with recent new directions in force field design and machine learning of potential energy surfaces showing promising results(16, 93–100). Improved accuracy in sampling can potentially be achieved by including nuclear quantum effects or electronic quantum effects through techniques such as path integral MD (101–104) or ab initio MD (105–108), respectively. All of these MD methods include vibrational sampling along the potential, however, the overall shape of an ensemble linear absorption spectrum is incorrect without the vibronic contributions (although the standard deviation of the ensemble and Franck-Condon spectrum should agree in the limit of identical solvent broadening and the two spectra will be identical in the limit of infinite temperature). Another challenge in including environmental effects in optical spectroscopy simulations is that often there is a mismatch in the Hamiltonians used to sample configurations (perhaps a classical force field to achieve desired time scales) and to compute the electronic excited states (wherein the electrons must be treated quantum mechanically). This mismatch in Hamiltonians causes inaccuracies in the computed spectral densities and optical spectra (109–114). In addition to altering the spectrum for a single optical excitation, the molecular environment could cause higher lying electronic states to mix with a low-lying bright state. This state mixing effect can likely only be captured through an MD simulation that allows for interaction of the chromophore with an atomistic environment and for the chromophore to explore regions of the potential away from the ground state minimum. Overall, properly including the environment along with vibronic effects is a long-standing challenge for accurate simulations of optical spectroscopy.

Both vibronic and environmental effects are clearly important for capturing accurate spectral energies, shapes, and time-dependent features, but until relatively recently(30, 38, 88, 89, 109, 115–120), theorists would generally choose either vibronic *or* environmental effects to include in spectral simulations. We seek to answer the question ‘How can vibronic and environmental effects be combined in simulations of optical spectroscopy?’ In this review we present recent work that follows two directions for combining these important effects for both linear and nonlinear optical spectroscopy: (1) a static approach employing only the static input of independent configurations that combines the harmonic model with ensemble sampling and (2) a dynamic approach employing a correlated time-series of configurations that is based on a cumulant expansion of the linear and nonlinear response function generated from correlation functions(121, 122). We first provide a brief overview of the two directions, highlighting important distinctions between the two methods and how the calculations are performed in practice, before going into more detail about and showing

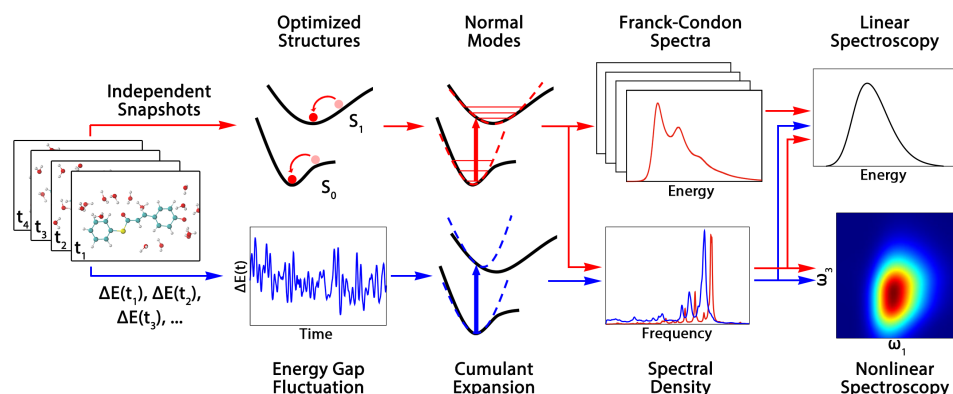


Figure 2

Schematic outlining two approaches for generating linear and nonlinear optical spectra that combine vibronic and environmental effects: the static approach to combine ensemble sampling with a harmonic model (red lines) and the dynamic approach based on computing the energy gap fluctuations of the fully coupled chromophore-environment system (blue lines). In this schematic the data shown is for the deprotonated *trans*-thiophenyl-*p*-coumarate (pCT⁻) chromophore in water.

results from each method.

2. Theoretical Background

The schematic in **Figure 2** outlines the static and dynamic approaches for combining vibronic and environmental effects in linear and nonlinear optical spectroscopy that we focus on in this review article. Both methods begin by simulating a chromophore within its atomistic environment at room temperature. In practice, this simulation is usually an MD trajectory, which will provide either the independent snapshots of atomic positions spaced apart in time needed for the static approach, or will provide a time-sequence of configurations that will be used to compute ground to excited state energy gaps for the dynamic approach.

We first outline the scheme for the static approach, shown with red lines in **Figure 2**. For each independent snapshot sampled from the ensemble, we assume a separation of timescales for the nuclear redistribution of the environment upon electronic excitation of the chromophore to justify freezing the atomistic environment during a geometry optimization of the chromophore in its ground S_0 and excited S_1 states. At these optimized geometries the normal modes are computed within a harmonic approximation to the potential energy surfaces and the frequencies, displacements, and relative rotations between ground and excited state normal modes are used to compute a Franck-Condon spectrum by parametrizing a harmonic model called the generalized Brownian oscillator model (GBOM) (37, 123). This model assumes displaced harmonic ground and excited state potential energy surfaces that can have different curvatures and that may be rotated to mix the normal modes of the ground and excited state, known as a Duschinsky rotation (124).

In the GBOM, the nuclear Hamiltonians for the electronic ground and excited state with N_j vibrational modes can be written as:

GBOM: Generalized Brownian oscillator model, a nuclear model Hamiltonian obtained from a harmonic expansion of the ground and excited state potential energy surfaces around their minima.

Duschinsky rotation: Rotation matrix relating the ground and excited state normal modes.

$$H_g(\hat{\mathbf{q}}_g, \hat{\mathbf{p}}_g) = \frac{1}{2} \sum_j^{N_j} [\hat{p}_{g,j}^2 + \omega_{g,j}^2 \hat{q}_{g,j}^2], \quad 1a.$$

$$H_e(\hat{\mathbf{q}}_e, \hat{\mathbf{p}}_e) = \frac{1}{2} \sum_j^{N_j} [\hat{p}_{e,j}^2 + \omega_{e,j}^2 \hat{q}_{e,j}^2] + \Delta_{eg}^0, \quad 1b.$$

where $\hat{\mathbf{q}}_g$ is the operator of nuclear coordinates and $\hat{\mathbf{p}}_g$ is the operator of momentum on the ground state PES and where the ground and excited state normal modes are related through the linear transformation:

$$\hat{q}_{g,i} = \sum_j^{N_j} J_{ij} \hat{q}_{e,j} + K_i. \quad 2.$$

cumulant expansion:
Used to reformulate a quantum statistical average of the time-ordered exponentials in terms of an expansion of cumulants: mean, variance, third central moment, etc.

Here, K_i is the shift vector describing the displacement between ground and excited state PES minima, Δ_{eg}^0 is the adiabatic energy gap between the surfaces, and \mathbf{J} is the Duschinsky rotation matrix. The parametrized GBOM can then be used to generate optical spectroscopy data in two different ways. Within the Condon approximation, the linear absorption spectrum of the GBOM can be solved exactly, leading to a Franck-Condon spectrum within a single specific environment configuration. These spectra can then be summed in various ways, as described in the next section, to create a linear absorption spectrum that captures both vibronic and environment effects. Alternatively, the harmonic GBOM can be used to generate a spectral density in which the vibrational modes that couple to the optical excitation are computed in the presence of the specific environment, as seen in **Figure 1b**.

Key to this alternative route for the static approach, as well as the dynamic approach outlined below, is the ability to write the response functions in terms of a cumulant expansion of the energy gap fluctuation operator $\delta U(\hat{\mathbf{q}}_g)$. The linear response function can then be written as(121)

$$\begin{aligned} \sigma(\omega) &\propto \text{Re} \int_0^\infty dt e^{i(\omega - \bar{\omega}_{eg})t} \left\langle \exp_+ \left[-i \int_0^t d\tau \delta U[\hat{\mathbf{q}}_g(\tau)] \right] \right\rangle \\ &\propto \text{Re} \int_0^\infty dt e^{i(\omega - \bar{\omega}_{eg})t} \exp \left[\sum_{n=2}^\infty g_n(t) \right]. \end{aligned} \quad 3.$$

Here, $\bar{\omega}_{eg} = \langle U(\hat{\mathbf{q}}_g) \rangle$ is the thermal average of the energy gap operator connecting the electronic ground state g to the excited state e , $g_n(t)$ is the n^{th} order cumulant and Hartree atomic units are used throughout. For the GBOM, the thermal average can be evaluated analytically as(37)

$$\bar{\omega}_{eg} = \Delta_{eg}^0 + \frac{1}{2} \sum_{jnm} K_m J_{mj}(\omega_{e,j})^2 J_{jn}^T K_n + \sum_{jn} \frac{1}{4\omega_{g,n}} [J_{nj}(\omega_{e,j})^2 J_{jn}^T - (\omega_{g,n})^2] \coth \left(\frac{\beta\omega_{g,n}}{2} \right), \quad 4.$$

where $\beta = 1/(k_B T)$. The thermal average $\bar{\omega}_{eg}$ reduces exactly to the vertical excitation energy of snapshot j evaluated at the ground state optimized geometry if the ground and excited state frequencies of the GBOM are identical and no Duschinsky effects are considered.

The cumulants of both the linear and nonlinear response functions can be expressed in terms of time-ordered integrals of increasing orders of quantum time-correlation functions

Quantum and classical correlation functions

Computing exact quantum correlation functions requires the full knowledge of the eigenstates of the nuclear Hamiltonian and they are therefore generally only accessible for simple model systems, such as harmonic oscillators. Classical correlation functions are much simpler to calculate and can, for example, be constructed from a set of correlated configurations extracted from a molecular dynamics trajectory. For this reason, much work has been focused on deriving approaches to approximately reconstruct the quantum correlation function from its classical counterpart.(125–128) This can be achieved through a quantum correction factor, which can be derived, for example, by exploiting that the classical and the quantum correlation functions must agree in the high temperature limit.

$C_{\delta U}$ of the energy gap fluctuation operator $\delta U = U - \bar{\omega}_{eg}$. For the GBOM, these quantum time-correlation functions have analytical expressions(37), but these quantum correlation functions are not available for realistic systems. For the second order cumulant

$$g_2 [C_{\delta U}^{\{2\}}] (t) = \int_0^t d\tau_2 \int_0^{\tau_2} d\tau_1 C_{\delta U}^{\{2\}}(\tau_2 - \tau_1), \quad 5.$$

where

$$C_{\delta U}^{\{2\}}(t) = \langle \delta U(t) \delta U(0) \rangle, \quad 6.$$

with analogous expressions for higher order cumulants(129). If a system possesses Gaussian fluctuations of the energy gap, the cumulant expansion at second order is exact and all higher order cumulant terms are zero.

Truncating the cumulant expansion at second order maps the system dynamics onto a fictitious bath of linearly coupled harmonic oscillators that possess Gaussian energy gap fluctuations, for which linear and nonlinear spectroscopy signals can be computed analytically(121). The second order cumulant contribution $g_2(t)$ is a functional of the electronic-vibrational coupling described by the spectral density $\mathcal{J}(\omega)$, computed by switching into Fourier space and evaluating the time-ordered integrals analytically(121):

$$g_2(t) = \frac{1}{\pi} \int_0^\infty d\omega \frac{\mathcal{J}(\omega)}{\omega^2} \left[\coth\left(\frac{\beta\omega}{2}\right) [1 - \cos(\omega t)] - i[\sin(\omega t) - \omega t] \right], \quad 7.$$

where

$$\mathcal{J}(\omega) = i\theta(\omega) \int dt e^{i\omega t} \text{Im} C_{\delta U}(t). \quad 8.$$

A similar expression can be derived(37) for the third order correction $g_3(t)$. Within the GBOM, both the difference in curvature, with $\omega_{g,i} \neq \omega_{e,i}$, and the Duschinsky rotation lead to a nonlinear dependence on nuclear coordinates of the operator $\delta U(\hat{\mathbf{q}}_g)$ and thus non-Gaussian energy gap fluctuations, meaning that truncation of cumulant expansion at second order cumulant is no longer exact(37).

Although a truncated cumulant expansion, unlike the Franck-Condon approach, introduces approximations in the linear absorption spectrum when applied to the GBOM, it allows for the straightforward computation of nonlinear optical spectra based on the third order response function, for which exact closed-form expressions for the GBOM Hamiltonian are not currently available. For example, in the second order cumulant approximation,

Gaussian fluctuations: Energy gap fluctuations resulting from a Gaussian process possess a Gaussian energy gap distribution and multivariate Gaussian joint distributions at different time points. For such Gaussian dynamics, the optical spectrum can be expressed exactly in a second order cumulant expansion.

the absorptive two-dimensional electronic spectroscopy signal for a two-level system can be written as

$$S_{2\text{DES}}(\omega_3 - \bar{\omega}_{\text{eg}}, t_{\text{delay}}, \omega_1 - \bar{\omega}_{\text{eg}}) \propto \text{Re} \int_0^\infty dt_3 \int_0^\infty dt_1 \left[e^{i\omega_3 t_3 + i\omega_1 t_1} (R_1(t_3, t_{\text{delay}}, t_1) + R_4(t_3, t_{\text{delay}}, t_1)) \times e^{-i\omega_3 t_3 + i\omega_1 t_1} (R_2(t_3, t_{\text{delay}}, t_1) + R_3(t_3, t_{\text{delay}}, t_1)) \right], \quad 9.$$

where $R_1 - R_4$ are contributions from individual double-sided Feynman diagrams that, under the second order cumulant approximation, are completely specified by $g_2(t)$ (121).

Within this lower branch of the static approach shown in **Figure 2**, the inhomogeneous broadening of the environment can be accounted for with the addition of phenomenological solvent broadening, and the spectral density can then be used to compute the linear spectrum or nonlinear spectra, such as the two-dimensional electronic spectrum (2DES) and transient absorption spectrum. These spectra will be missing some of the explicit environment effects that manifest in the low-frequency region of the spectral density(92), but will contain the effects of how the explicit solvent affects the high-frequency chromophore vibrations. Because nonlinear optical spectroscopy generally follows the evolution of an excited state over time, the separation of timescales argument that justifies the use of a frozen environment for normal mode calculation will be more valid at shorter timescales and will degrade over time as the nuclear response of the environment to the electronic excitation becomes important.

The scheme for the dynamic approach for using the linear and nonlinear response function is shown with blue lines in **Figure 2**. For a time-series of chromophore-environment configurations, the energy gap is computed to generate the energy gap fluctuations as a function of time. The cumulant expansion of the energy gap fluctuation operator can then be used in linear and nonlinear response theory, with truncation of the expansion at second order mapping the energy fluctuations onto harmonic ground and excited state surfaces (note that these harmonic surfaces are not the same as those used in the GBOM wherein the harmonic surfaces are expanded around the minimum). From this harmonic mapping, the spectral density can be computed but, unlike for the static approach, the full coupling to the environment is included in this spectral density, manifesting in spectral weight in the low-frequency region(92). From the spectral density, both the linear and nonlinear spectra can be generated, with movement of the chromophore and the environment treated on equal footing, thus naturally including both vibronic and environment effects.

In the remainder of this review we go deeper into the theory of these two approaches and highlight results of some recent studies using both methods.

3. Static input approach: Combining ensemble sampling with the harmonic model for linear and nonlinear spectroscopy

Recently, two of the authors introduced an approach for simulating linear spectroscopy that combines ensemble sampling of chromophore-environment configurations with the vibronic effects captured within the Franck-Condon approach(90). This approach, requiring only static input, follows the top path in the scheme in **Figure 2** by summing over multiple Franck-Condon (FC) spectra that sample different minima due to interactions with the

2DES:

Two-dimensional electronic spectroscopy, a nonlinear optical spectroscopy method for measuring ultrafast phenomena showing correlation between excitation, ω_1 , and emission, ω_3 , frequencies.

specific environment.

For each frame in the ensemble, the spectrum depends on the coordinates of the chromophore and the solvent environment $\mathbf{R}_j = \{\mathbf{R}_j^c, \mathbf{R}_j^s\}$, where \mathbf{R}_j^c is the chromophore degrees of freedom and \mathbf{R}_j^s is the solvent degrees of freedom. Following the assumption that the solvent nuclear degrees of freedom are slower than the degrees of freedom of the chromophore on the time scale of optical transition, a Franck-Condon spectrum is computed by optimizing the ground and excited state of the chromophore, thereby determining \mathbf{R}_j^c within frozen solvent environment \mathbf{R}_j^s . For a given frame, the FC spectrum will then be computed by integrating the ground and excited state vibrational wave functions of the chromophore over \mathbf{R}_j^c variables while being parametrically dependent on \mathbf{R}_j^s variables. To combine vibronic and environment effects, the absorption spectrum is then given by a sum over individual FC spectra as

$$\sigma_{\text{sum-FC}}(\omega) = \frac{1}{N_{\text{frames}}} \sum_j^{N_{\text{frames}}} \sigma_{\text{FC},j}(\omega), \quad 10.$$

where σ_{FC} is a Franck-Condon spectrum of the chromophore for a given nuclear configuration of solvent obtained from a single MD frame,

$$\sigma_{\text{FC}}(\omega) = \frac{4\pi^2}{3c} |\boldsymbol{\mu}_{\text{eg}}|^2 \sum_{v_g} \rho_{v_g} \sum_{v_e} \left[|\langle \phi_{v_g} | \phi_{v_e} \rangle|^2 [\omega_{v_e} - \omega_{v_g}] \mathcal{N}(\omega - [\omega_{v_e} - \omega_{v_g}]) \right]. \quad 11.$$

The terms ϕ_{v_g} and ϕ_{v_e} denote nuclear vibrational wave functions and ω_{v_e} and ω_{v_g} represent the corresponding energy of the system in vibronic states $|g v_g\rangle$ and $|e v_e\rangle$. The temperature-dependent Boltzmann population ρ_{v_g} determines the population of the ground vibrational states. The integral $\langle \phi_{v_g} | \phi_{v_e} \rangle$ is the Franck-Condon overlap that determines the intensity of the vibronic transition between different vibrational levels. The total area of each FC spectrum in the sum is determined by value of the transition dipole moment $\boldsymbol{\mu}_{\text{eg}}$ squared. The spectrum can be broadened using Gaussian functions, \mathcal{N} , centered at the transition energies with a width to account for finite sampling. Alternatively, the broadening can also be introduced through an effective low frequency spectral density of the Debye form(37).

Since publishing that work, versions of this approach have been used by Sharifzadeh and co-workers to model the spectrum of stacked organic chromophores with multiple low-energy minima (62) and by Santoro and co-workers to model flexible chromophores in solution(118). Both of these studies made use of a vertical gradient or Hessian approach that avoids optimizing the geometry of the excited state and therefore decreases the computational cost of computing the Franck-Condon spectra(130).

An alternative cost-saving strategy that we introduced uses an average Franck-Condon spectrum along with a separation of temperature regimes for the solvent and chromophore.(90) This approach, which we call ensemble- average zero temperature Franck-Condon (E-avg-ZTFC), computes the excitation energies for an ensemble of MD configurations at the desired temperature to capture chromophore-environment interactions and then dresses each of these excitation energies with an average zero-temperature Franck-Condon spectrum that has been computed for a few snapshots in the presence of a frozen environment. With this technique, the computed excitation energies each weighted by the corresponding oscillator strength are identical to an ensemble spectrum, containing the full temperature dependence of the system. Dressing each of these states with a Franck-Condon spectrum replaces the Gaussian function that is usually used in the generation of an en-

Franck-Condon (FC) spectrum: Linear spectrum wherein the intensity of vibronic transitions is proportional to the square of the overlap of ground and excited state vibrational wave functions

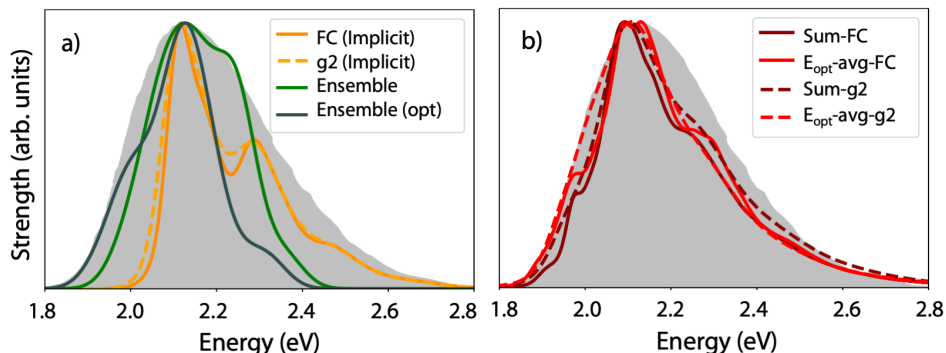


Figure 3

Experimental(131) (gray) and simulated absorption spectra for the Nile red chromophore in the water, with the maximum intensity aligned for all spectra. The explicit solvent results are averaged over 45 MD snapshots. Equivalent broadening was used for all spectra. (a) Vibronic spectra for the structure optimized in implicit solvent are computed in the Franck-Condon (FC) approach or second order cumulant approximation (g_2). Ensemble spectra computed directly from MD snapshots and where the chromophore has been optimized in a frozen explicit solvent environment. (b) Four ways to combine vibronic and environment effects within the static approach. Solid lines show spectra computed using a sum of finite-temperature Franck-Condon spectra computed within explicit solvent environment and using an average Franck-Condon spectrum convoluted with the ensemble optimized spectrum ($E_{opt-avgFC}$). Dashed lines show spectra computed using a sum of cumulant based spectra and using an average vibronic shape function ($E_{opt-avg-g_2}$).

semble spectrum, but adds a correction to the spectral shape for vibronic transitions and zero-point energy. The computational cost of this method is similar to that of computing an ensemble spectrum, but the spectral shape will be improved. This method is not suitable for modeling the spectra of systems with significant vibronic fine structure, as the peaks will be overly broadened by the ensemble sampling, and is instead better for chromophores with strong interactions with the environment. Our original implementation of the E-avg-ZTFC method double counts the chromophore degrees of freedom by sampling the chromophore vibrational modes in the MD sampling and the zero-point motion of the chromophore in the Franck-Condon spectrum. Our follow up paper working with Markland and co-workers outlines how this double counting can be removed.(37)

We will here introduce another method that combines ensemble sampling of the environment with Franck-Condon calculations that we plan to discuss in more detail in a future publication. This method avoids the double counting of chromophore zero point energy that was present in the original E-avg-ZTFC method, and its computational cost is between that of the E-avg-ZTFC method and the method that computes a Franck-Condon spectrum for every configuration. Like the E-avg-ZTFC method, it uses an average Franck-Condon spectrum computed for a few snapshots in the presence of the frozen explicit environment, but instead of using this spectrum to dress the excitation energies of the MD configurations, it will dress the excitation energies of structures where the chromophore has been optimized in the ground state within the frozen environment. By optimizing the geometry of the chromophore within the frozen environment, we remove the temperature from the chromophore degrees of freedom but keep the temperature induced environmental effects (such

as the environment leading to twisted configurations that would not be sampled at zero temperature). **Figure 3a** shows the computed ensemble and optimized ensemble spectrum for the Nile red chromophore in water, where we see that the ensemble spectrum for the chromophore optimized in explicit solvent is more narrow because the temperature is removed from the chromophore degrees of freedom. Neither of the ensemble spectra show good agreement with the shape or width of the experimental spectrum.

To add vibronic effects to the computed ensemble optimized spectrum, we no longer use a zero-temperature Franck-Condon spectrum, but instead use an average finite temperature Franck-Condon spectrum so that the temperature effects of the environment are treated classically with MD sampling and that of the chromophore are treated quantum mechanically by population of quantized vibrational energy levels. In this approach, in Eq. 9, only the transition dipole moment and transition energy retain dependence on solvent degrees of freedom. The resulting expression for the absorption spectrum is

$$\sigma_{\text{Eopt-avg-FC}}(\omega) \propto \frac{1}{N_{\text{frames}}} \sum_j^{N_{\text{frames}}} |\mu_{\text{eg},j}|^2 \sigma_{\text{FC}}^{\text{avg}}(\omega - \Delta\omega_{\text{eg},j}) \quad 12.$$

where $\Delta\omega_{\text{eg},j} = \omega_{\text{eg},j} - \omega_{\text{eg}}^{\text{avg}}$. The vertical excitation energy for frame j is $\omega_{\text{eg},j}$ as computed for the ground state optimized geometry of the chromophore in the frozen solvent environment, and $\omega_{\text{eg}}^{\text{avg}}$ is the vertical excitation energy averaged over N_{frames} . The average vibronic shape function $\sigma_{\text{FC}}^{\text{avg}}$ is computed by averaging over finite temperature Franck-Condon spectra calculated in a frozen solvent environment, where all spectra are shifted such that their vibronic 0-0 transitions are aligned. The average vibronic shape function is normalized so that it integrates to one, with the sum in Eq. 12 then weighting each vibronic shape function by the transition dipole moment squared of the optimized frozen solvent snapshot, thus accounting for some non-Condon effects.

Depending on how many configurations are included in the average FC spectrum, this method of combining ensemble optimized structures with a finite-temperature FC spectrum, or Eopt-avg-FC, is computationally much more efficient than those that compute an excited state optimized structure or gradient or Hessian for each configuration. In practice, we have found that an average over ten configurations is adequate for simulating the average FC spectra for chromophores in solution, whereas we find that on the order of a hundred to a thousand configurations is needed for sampling the ensemble. For the case of the Nile red chromophore in water, the FC spectra computed in explicit solvent in **Figure 1a** shows some variation in the height of the 0-0 vibronic peak across configurations, but the overall shape of the FC spectrum does not change significantly. The validity of an average FC spectrum can be tested by computing the spectrum for configurations that appear to sample different minima, e.g. a planar and twisted configuration of a chromophore, and then using different average FC spectra as needed.

The absorption spectrum computed with the new Eopt-avg-FC method shows good agreement with the more expensive method of summing a different FC spectrum for each configuration, see **Figure 3b**. Both methods capture the asymmetry of the spectrum and the high-energy vibronic tail, with the Eopt-avg-FC spectrum being a bit broader than the summed FC spectrum. Compared to experiment, both methods are a bit too narrow at the top of the spectrum, which could be due to limited sampling (only 45 snapshots) or the shape of the FC spectrum obtained with the chosen electronic structure method. We note that even better agreement with the experimental spectrum could be obtained with a different electronic structure method, as these computational results used CAM-

B3LYP (132) computed within the Tamm-Dancoff approximation, but we found improved agreement with the experimental spectrum without the Tamm-Dancoff approximation and using the larger 6-311G** basis set.

As noted in the scheme in **Figure 2**, the GBOM approach for which the Franck-Condon spectrum generates the exact linear absorption spectrum can instead be used to compute a response function and spectral density within the second order cumulant approximation. (37) Figure 1a compares the computed spectra for these two approaches as generated from the GBOM parametrized from the Nile Red chromophore in implicit water solvent. The spectra have similar shapes, but the exact FC spectrum has slightly more vibronic fine structure than the spectrum generated with the second order cumulant approximation. This result is in agreement with our previous work that showed that the addition of third order cumulant term sharpens the vibronic fine structure, bringing the spectrum closer to the exact FC result. Although the second order cumulant approximation introduces an additional approximation beyond the FC method, and therefore does not generate an exact absorption spectrum for the GBOM, the second order cumulant response functions provide a route to nonlinear spectroscopy within the static approach. We therefore here formulate equivalents of the sumFC and the Eopt-avg-FC schemes in the cumulant approach, which we denote as sum-g2 and Eopt-avg-g2 respectively. For linear spectroscopy, we can sum the response functions obtained within the second order cumulant expansion g_2 to obtain

$$\sigma_{\text{sum-g2}}(\omega) = \frac{1}{N_{\text{frames}}} \sum_j^{N_{\text{frames}}} \sigma_{g2,j}(\omega) \quad 13.$$

with the response function for a given frame j given by

$$\sigma_{g2}(\omega) = \frac{4\pi^2\omega}{3c} |\boldsymbol{\mu}_{\text{eg}}|^2 \text{Re} \int_0^\infty \exp[i(\bar{\omega}_{\text{eg}} - \omega)t - g_2(t)] dt \quad 14.$$

where the second order cumulant g_2 , the thermal average of the energy operator for the GBOM $\bar{\omega}_{\text{eg}}$, and the transition dipole moment $\boldsymbol{\mu}_{\text{eg}}$ all depend parametrically on the frozen solvent environment.

For the more simplified Eopt-avg-g2 scheme, the linear spectrum can be computed as

$$\sigma_{\text{Eopt-avg-g2}}(\omega) \propto \frac{1}{N_{\text{frames}}} \sum_j^{N_{\text{frames}}} |\boldsymbol{\mu}_{\text{eg},j}|^2 \sigma_{g2}^{\text{avg}}(\omega - \Delta\omega_{\text{eg},j}) \quad 15.$$

where the definition of $\Delta\omega_{\text{eg},j}$ is the same as for the Franck-Condon based approach and σ_{g2}^{avg} is an averaged vibronic shape function in the second order cumulant approach computed for a set of GBOMs in frozen solvent environment, where the averaging is carried out by shifting the 0-0 transitions of all GBOM spectra to the average 0-0 transition energy. Furthermore, as in the FC-based approach, the average shape function is normalized such that it integrates to one.

The resulting linear absorption spectra for these two approximate cumulant based approaches are shown in **Figure 3b**. Similar to what we see in **Figure 3a** for the implicit solvent calculation, the second order cumulant spectra are broader and have less fine structure than their FC based counterparts, which in this case leads to fortuitous better agreement with the experimental absorption spectrum. Similar to the FC based methods, the spectra computed using a sum or using an average vibronic spectrum placed at the energies of the

ground state optimized structures are in good agreement with each other, suggesting that the use of the average response function may be a valid way to reduce computational cost.

Although the sum-g2 and the Eopt-avg-g2 schemes introduce additional approximations in linear spectroscopy when compared to their Franck-Condon based counterparts, they can be straightforwardly extended to the computation of nonlinear spectra, such as 2DES. The corresponding expressions are given by

$$S_{\text{sum-g2}}(\omega_3, t_{\text{delay}}, \omega_1) = \frac{1}{N_{\text{frames}}} \sum_j^{N_{\text{frames}}} S_{2\text{DES},j}^{g2}(\omega_3, t_{\text{delay}}, \omega_1), \quad 16.$$

and

$$S_{\text{Eopt-avg-g2}}(\omega_3, t_{\text{delay}}, \omega_1) \propto \frac{1}{N_{\text{frames}}} \sum_j^{N_{\text{frames}}} |\mu_{\text{eg},j}|^4 S_{2\text{DES}}^{g2,\text{avg}}(\omega_3 - \Delta\omega_{\text{eg},j}, t_{\text{delay}}, \omega_1 - \Delta\omega_{\text{eg},j}), \quad 17.$$

where $S_{2\text{DES}}^{g2,\text{avg}}$ denotes an average 2DES shape function computed for a number of frozen solvent snapshots, where the averaging is carried out by shifting all spectra such that the 0-0 transitions coincide with the average 0-0 transition, and the resulting averaged spectrum is again normalized to integrate to one and then scaled by the transition dipole moment to the fourth power for each frame.

Using the same parameters as for the linear absorption spectra based on the second order cumulant approximation presented in **Figure 3**, the corresponding 2DES results are shown in **Figure 4**. As might be expected from the implicit solvent results that we know from **Figures 1** and **3** over-emphasize the vibrational-electronic coupling, the implicit solvent 2DES shows more narrow features and more clear off diagonal features indicative of vibronic coherences. The 2DES containing vibronic and environment effects are broader and appear to show faster electronic relaxation. The good agreement between the sum and average linear response function methods from the linear absorption spectra is maintained in the 2DES, at least at the time scales examined here.

Although combining the GBOM with the cumulant expansion provides a route to simulation of nonlinear spectroscopy, the method has not yet been thoroughly benchmarked with either experiment or with the dynamic approach described below. Proper comparisons of the dynamic and static approaches for combining vibronic and environment effects requires performing the MD at the same level of the theory as the excited state calculations to avoid artifacts due to the mismatch in Hamiltonians. Loco et al. (88) have performed a study comparing similar versions of the static and dynamic approaches presented here in the context of absorption lineshapes. Compared to the static approaches outlined here, the dynamic approach we next describe likely provides a more rigorous route to nonlinear spectroscopy because of the full dynamic coupling of the chromophore to the environment, removing the separation of time scales approximation, as we describe in the next section.

4. Dynamic input approach: Energy gap fluctuations and the cumulant expansion for linear and nonlinear spectroscopy

The dynamic approach highlighted here based on the Kubo formalism (133–135) for modeling linear and nonlinear optical spectroscopy uses a time-series of excitation energies to compute linear and nonlinear correlation functions. One of the main advantages of this approach is that all relevant physical phenomena arising from movement of the atoms of

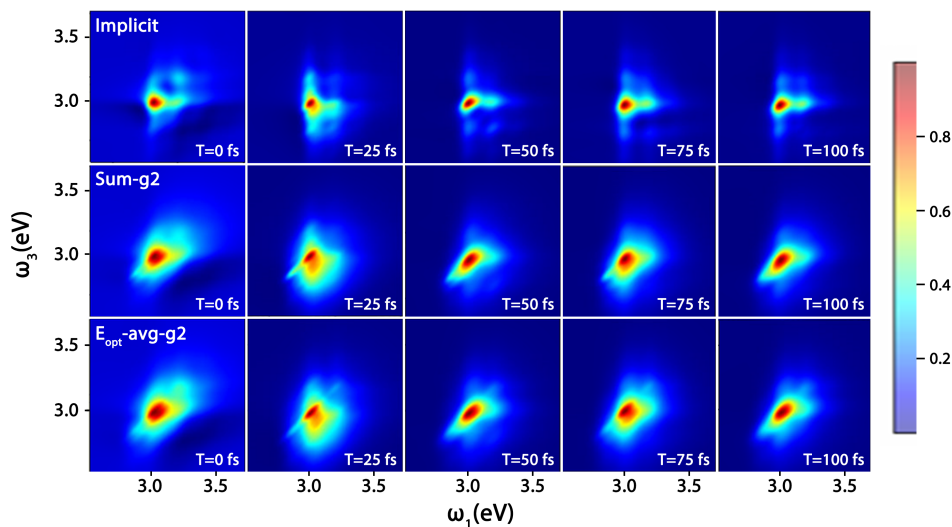


Figure 4

Comparison of three methods to simulate 2D electronic spectra within the static approach for the Nile red chromophore in water where the absorption maxima have been energetically aligned to facilitate comparisons of spectral shapes. The implicit solvent results are based on the optimized ground and excited state structures in continuum solvent. The other methods based on a second order cumulant approximation combine vibronic and environment effects within a static picture by including data from the same 45 snapshots of Nile Red optimized in explicit solvent used in Figures 1 and 3. The average response function approach shows good agreement with the more rigorous approach that sums the response functions.

the chromophore and the environment are included on equal footing, invoking no separation of timescales for the chromophore and environment. For a large, disordered system, this time-series approach also has the advantage of avoiding geometry optimization of system, instead sampling many local minima and potentially anharmonic regions of the potential energy surfaces.

Except for simple model systems, the exact quantum correlation functions $C_{\delta U}^{\{n\}}$ are inaccessible. However, approximately reconstructing quantum correlation functions from their classical counterparts $C_{\delta U}^{\{n\},cl}$ is possible using quantum correction factors.(125–128) Classical correlation functions are much easier to compute than their quantum counterparts and can, for example, be constructed by calculating vertical excitation energies along an MD trajectory(20, 21, 24–26, 88, 92, 109, 136), as outlined by the blue lines in the scheme in **Figure 2**. In a recent study by two of the authors working with Markland and co-workers, we showed that a truncated cumulant expansion of the energy gap fluctuations combined with a QCF provides a highly appealing approach for simulating optical spectra since it accurately captures vibronic and environmental effects for both strong and weak solvent interactions(37).

We recently demonstrated that the quantum mechanical (QM) electronic polarization of the environment within the excited state calculation affects the spectral densities and lineshapes within the cumulant framework. (92) We found that the QM environment can enhance or depress the coupling of fast chromophore degrees of freedom to the energy

QM: Quantum mechanical, electrons are treated quantum mechanically within the electronic structure calculations

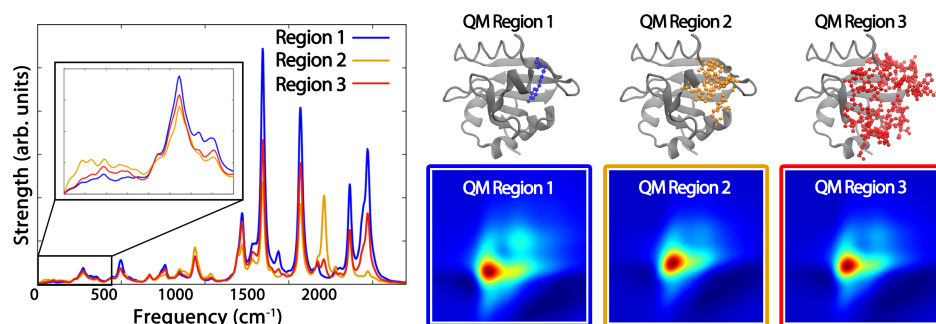


Figure 5

The spectral density and time=0 2DES for photoactive yellow protein as computed for a 6 ps MD trajectory, where the CAM-B3LYP/6-31G* excited state calculations were performed with three different QM regions.

gap, altering the electronic-vibrational coupling and the resulting vibronic progressions in the absorption spectrum. For chromophores in solution, the changes in spectral density peak heights were systematic with increasing QM region size, converging after inclusion of approximately one full solvation shell, and generally adding more weight to the low-frequency region of the spectral density, resulting in a broader linear absorption spectrum and faster decay time in the 2DES. However, for the chromophore inside of photoactive yellow protein, changes in the spectral density were not systematic with increasing QM region size, see **Figure 5**. Including only the chromophore as QM and surrounding protein as fixed point charges, as in QM region 1, leads to more intense high-frequency peaks, resulting in more vibronic fine structure in the linear absorption spectrum and more intense signals of vibronic coherences in the 2DES. Including some nearby protein residues around the chromophore in the QM region, as in QM region 2, leads to enhancement of the low-frequency region of the spectral density, removing some of the vibronic fine structure from the linear absorption spectrum, but the QM treatment of the entire hydrophobic protein pocket around the chromophore, as in QM region 3, yields spectral shapes between those of QM regions 1 and 2. Key to these spectral differences is how the QM treatment of the environment affects the low-frequency region of the spectral density. These differences in the specific environment seen in the low-frequency region cannot be captured with the static approaches described previously that freeze the atomistic environment during the normal mode computations. With the choice of QM region clearly affecting the optical spectra and with increasing QM region leading to a large increase in computational cost, it is unclear if QM treatment of the environment or extended sampling of configuration space will be more important, and the answer is likely system dependent.

Although thus far within the dynamic approach we have focused on results that truncate the cumulant expansion at second order, our recent studies suggest that the addition of the third order term can improve the computed linear absorption spectrum and can capture some of the nonlinear coupling effects on the 2DES caused by Duschinsky mode mixing and the differing curvatures of the ground and excited state potentials(137). We found that the third order cumulant correction is strongly dependent on the QM treatment of the solvent environment, revealing the interplay between environmental polarization and the

electronic-vibrational coupling.

With excitation energies computed for a long enough MD trajectory, all of configuration space could be sampled and the convergence of correlation functions that enter into the linear and nonlinear response functions would be straight-forward. However, in practice computing the excitation energies for such a lengthy trajectory may be impossible and the question then arises about how best to generate the optical spectra obtained within the dynamic approach.

A potential way to sample both the fast chromophore degrees of freedom responsible for vibronic coherences and the slow conformational changes of the environment giving rise to spectral broadening is to use the information obtained from several short uncorrelated MD trajectories. Data from multiple trajectories can then be combined in a number of different ways. One approach is to compute a spectrum for each individual trajectory and sum the spectra. The resulting expression for linear and nonlinear spectroscopy is highly analogous to the sum-g2 approach introduced in Eqns. 13 and 16, with the difference that the cumulants, thermal averages of the energy gap, and average dipole moments are computed for individual MD trajectories, rather than for GBOMs in different frozen solvent environments. Alternatively, classical correlation functions of the energy gap computed for the individual trajectories can be averaged, such that

$$C_{\delta U, \text{avg}}^{\{2\}, \text{cl}}(t) = \frac{1}{N_{\text{traj}}} \sum_k^{N_{\text{traj}}} C_{U, k}^{\{2\}, \text{cl}}(t) - \left[\frac{1}{N_{\text{traj}}} \sum_k^{N_{\text{traj}}} \omega_{\text{eg}, k}^{\text{avg}} \right]^2 \quad 18.$$

where $C_{U, j}^{\{2\}, \text{cl}}(t)$ and $\omega_{\text{eg}, k}^{\text{avg}}$ are the classical autocorrelation function of the energy gap and the classical thermal average of the energy gap for trajectory k respectively. Averaging correlation functions as in Eqn. 18 yields a single, well-defined spectral density that includes both the effects of the fast degrees of freedom of the chromophore and conformational sampling of the environment. Eqn. 18 implicitly assumes a separation of timescales between the dynamic coupling of degrees of freedom captured by the correlation function of an individual trajectory and the slow moving environmental configurations sampled through the averaging over independent trajectories. However, for sufficiently long individual trajectories the average correlation function approach is expected to yield the same results as a correlation function computed from a single long trajectory, while providing a more computationally efficient way of sampling both slow and fast degrees of freedom. However, if a system possesses several distinct, long-lived conformations, for which the fast chromophore degrees of freedom couple differently to the energy gap, the sum-g2 approach provides a more accurate linear spectrum, as it allows for summing up the distinct spectral contributions from individual conformations, similar to the sum-FC approach.

One of the major drawbacks of this dynamic approach is the prohibitive cost of computing the lengthy time-sequence of electronic excitation energies required to converge the time correlation functions. Running thousands of excited state calculations, although expensive, is now computationally feasible with advanced high-performance computing clusters that can run hundreds of electronic structure calculations in parallel. Large scale excited state calculations that include a QM treatment of hundreds of atoms in the environment are now possible, for example time-dependent density functional theory is linear scaling (138, 139) as implemented in ONETEP(3) and is GPU accelerated as implemented in TeraChem.(1, 2, 4, 140) However, many thousands of these excited state calculations could potentially be avoided by instead using a smaller subset of excited state calculations

to train a machine learning algorithm to predict the excitation energies. In work where two of the authors collaborate with Markland and co-workers, we leverage the locality of chromophore excitations to develop machine learning models to predict the excited state energy gap of chromophores in complex environments for efficiently constructing linear and multidimensional optical spectra.⁽¹⁰⁰⁾ These models span a hierarchy of physical approximations, across a range of chromophore-environment interaction strengths, to provide different strategies for the construction of machine learning models that greatly accelerate the calculation of multidimensional optical spectra based on the dynamic approach. Given the promise of the dynamic approach for capturing vibronic and environmental effects on equal footing for simulations of optical spectroscopy, developing methods that build on the dynamic approach to make calculations faster and more accurate may be the next logical step in advancing simulations of linear and nonlinear spectroscopy.

5. Outlook

This review highlights recent advances in methods that combine vibronic and environmental effects in simulations of optical spectroscopy, touching briefly on how these effects manifest in optical linear and nonlinear spectra. Although these advances are promising in making strides towards simulating more complex condensed phase systems and making connections with experimental studies, there are still many improvements needed in the long road ahead.

The appeal of the static approach is avoiding the computation of a lengthy time-series of excitation energies. However, the static approach as discussed here does not capture dynamic coupling between the system and the environment and also approximates potential energy surfaces as being harmonic. Further advances will likely go beyond harmonic models to more directly capture the effects of realistic and complex potential energy surfaces. Although within the dynamic approach the inclusion of the third order term in the cumulant expansion captures some anharmonic effects, the behavior and accuracy of terms beyond second order cumulant remains relatively unexplored in realistic systems, and different dynamic approaches may be required to properly model systems with strongly anharmonic degrees of freedom.

Another relatively unexplored area is determining how accurate these methods are at longer timescales. These approaches are most valid at short timescales before the nuclei of the environment have a chance to respond to the electronic excitation, but it isn't clear at which timescales these methods will no longer be reliable.

Spectral density based approaches have been used to model the energy transfer in multi-chromophore systems, such as those performing light-harvesting, but the role of the effects discussed here on energy transfer is unclear. How will vibronic couplings and the treatment of the environment affect the electronic couplings and the energy transfer pathways?

The methods explored in this review are well-defined for two level systems and generally ignore higher lying transitions. However, realistic systems may have multiple chromophores transferring energy, may have environment-induced state mixings, will undergo state crossings, and presumably vibronic effects on excited state dynamics will be more pronounced due to excited-state absorption. Incorporating such nonadiabatic dynamics with vibronic and environmental effects remains a grand challenge in simulations of nonlinear optical spectroscopy. Ultimately, a bridge must be built between methods that capture vibronic and environment effects in condensed phase systems, and the advanced quantum dynamics approaches that more accurately treat nonadiabatic dynamics but are only affordable for

small systems.

SUMMARY POINTS

1. Vibronic and environmental effects can be combined in simulations of linear and nonlinear optical spectroscopy with either a static or dynamic approach.
2. Static approaches rely on a harmonic approximation to the ground and excited state potential energy surface within a frozen environment.
3. Dynamic approaches rely on truncation of a cumulant expansion and computation of energy gap correlation functions.
4. Compared to an implicit solvent model, explicit solvent not only broadens spectra, but also allows the solvent to couple to high-frequency chromophore modes in the spectral density.
5. The polarization and charge transfer provided by a QM treatment of the environment not only affects spectral peak positions, but also changes the couplings between the electronic excitation and nuclear vibrations.
6. Vibronic effects broaden the spectra via couplings with low-frequency solvent motions and generate vibronic peaks via couplings with high-frequency chromophore vibrations, both of which are influenced by the QM treatment of the environment.
7. Machine learning offers a promising route forward for pursuing the computationally expensive dynamic approach that treats the nuclear motion of the chromophore and environment on equal footing, truly combining vibronic and environment effects in modeling the spectroscopy of chromophores in complex environments.

DISCLOSURE STATEMENT

The authors are not aware of any affiliations, memberships, funding, or financial holdings that might be perceived as affecting the objectivity of this review.

ACKNOWLEDGMENTS

C. I. and L. S. are supported by the U.S. Department of Energy, Office of Science, Basic Energy Sciences, in the Computational and Theoretical Chemistry (CTC) and Condensed Phase and Interfacial Molecular Science (CPIMS) programs (Award DE-SC0019053), for improved methods for modeling functional transition metal compounds in complex environments: ground states, excited states, and spectroscopies. C. I. is also supported by the CTC program (Award DE-SC0020203) for developing new models of charge transfer, nonadiabatic dynamics, and nonlinear spectroscopy. Work in the Isborn group on development of static approaches for including vibronic and environmental effects in simulations of optical spectroscopy is supported by the NSF (CHE-1955656).

LITERATURE CITED

1. Isborn CM, Luehr N, Ufimtsev IS, Martínez TJ. 2011. Excited-state electronic structure with configuration interaction singles and Tamm–Dancoff time-dependent density functional theory on graphical processing Units. *J. Chem. Theory Comput.* 7:1814–1823

2. Isborn CM, Götz AW, Clark MA, Walker RC, Martínez TJ. 2012. Electronic absorption spectra from MM and ab initio QM/MM molecular dynamics: environmental effects on the absorption spectrum of photoactive yellow Protein. *J. Chem. Theory Comput.* 8:5092–5106
3. Prentice JC, Aarons J, Womack JC, Allen AE, Andrinopoulos L, et al. 2020. The ONETEP linear-scaling density functional theory program. *J. Chem. Phys.* 152:174111
4. Seritan S, Bannwarth C, Luehr N, Fales BS, Hohenstein EG, et al. 2020. TeraChem : accelerating electronic structure and ab initio molecular dynamics with graphical processing units. *J. Chem. Phys.* 152:224110
5. Warshel A, Levitt M. 1976. Theoretical studies of enzymic reactions: dielectric, electrostatic and steric stabilization of the carbonium ion in the reaction of lysozyme. *J. Mol. Biol.* 103:227–249
6. Gao J. 1996. Hybrid quantum and molecular mechanical simulations: an alternative avenue to solvent effects in organic chemistry. *Acc. Chem. Res.* 29:298–305
7. Senn HM, Thiel W. 2009. QM/MM methods for biomolecular systems. *Angew. Chem. Int. Ed.* 48:1198–1229
8. Curutchet C, Muñoz-Losa A, Monti S, Kongsted J, Scholes GD, Mennucci B. 2009. Electronic energy transfer in condensed phase studied by a polarizable QM/MM model. *J. Chem. Theory Comput.* 5:1838–1848
9. Olsen JM, Aidas K, Kongsted J. 2010. Excited states in solution through polarizable embedding. *J. Chem. Theory Comput.* 6:3721–3734
10. Caprasecca S, Curutchet C, Mennucci B. 2012. Toward a unified modeling of environment and bridge-mediated contributions to electronic energy transfer: a fully polarizable QM/MM/PCM approach. *J. Chem. Theory Comput.* 8:4462–4473
11. Olsen JMH, Steinmann C, Ruud K, Kongsted J. 2015. Polarizable density embedding: a new QM/QM/MM-based computational strategy. *J. Phys. Chem. A* 119:5344–5355
12. Bondanza M, Nottoli M, Cupellini L, Lipparini F, Mennucci B. 2020. Polarizable embedding QM/MM: the future gold standard for complex (bio)systems? *Phys. Chem. Chem. Phys.* :–
13. Hachmann J, Olivares-Amaya R, Jinich A, Appleton AL, Blood-Forsythe MA, et al. 2014. Lead candidates for high-performance organic photovoltaics from high-throughput quantum chemistry—the Harvard clean energy project. *Energy Environ. Sci* 7:698–704
14. Ramakrishnan R, Dral PO, Rupp M, Von Lilienfeld OA. 2015. Big data meets quantum chemistry approximations: The Δ -machine learning approach. *J. Chem. Theory Comput.* 11:2087–2096
15. Pereira F, Xiao K, Latino DARS, Wu C, Zhang Q, Aires-de Sousa J. 2017. Machine learning methods to predict density functional theory B3LYP Energies of HOMO and LUMO orbitals. *J. Chem. Inf. Model* 57:11–21
16. Butler KT, Davies DW, Cartwright H, Isayev O, Walsh A. 2018. Machine learning for molecular and materials science. *Nature* 559:547–555
17. Xia R, Kais S. 2018. Quantum machine learning for electronic structure calculations. *Nat. Commun.* 9:4195
18. Santoro F, Lami A, Improta R, Bloino J, Barone V. 2008. Effective method for the computation of optical spectra of large molecules at finite temperature including the Duschinsky and Herzberg–Teller effect: the Qx band of porphyrin as a case study. *J. Chem. Phys.* 128:224311
19. Bloino J, Biczysko M, Santoro F, Barone V. 2010. General approach to compute vibrationally resolved one-photon electronic spectra. *J. Chem. Theory Comput.* 6:1256–1274
20. Olbrich C, Strümpfer J, Schulten K, Kleinekathöfer U. 2011. Theory and simulation of the environmental effects on FMO electronic transitions. *J. Phys. Chem. Lett.* 14:1771–1776
21. Shim S, Rebentrost P, Valleau S, Aspuru-Guzik A. 2012. Atomistic study of the long-lived quantum coherences in the Fenna-Matthews-Olson complex. *Biophys. J.* 102:649–660
22. Baiardi A, Bloino J, Barone V. 2013. General time dependent approach to vibronic spectroscopy including Franck–Condon, Herzberg–Teller, and Duschinsky effects. *J. Chem. Theory*

- Comput.* 9:4097–4115
23. Mennucci B. 2015. Modeling absorption and fluorescence solvatochromism with QM/classical approaches. *Int. J. Quantum Chem.* 115:1202–1208
 24. Lee MK, Bravaya KB, Coker DF. 2017. First-principles models for biological light-harvesting: phycobiliprotein complexes from cryptophyte algae. *J. Am. Chem. Soc.* 139:7803–1814
 25. Mallus MI, Shakya Y, Prajapati JD, Kleinekathöfer U. 2018. Environmental effects on the dynamics in the light-harvesting complexes LH2 and LH3 based on molecular simulations. *Chem. Phys.* 515:141–151
 26. Blau SM, Bennett IG, Kreisbeck C, Scholes GD, Aspuru-Guzik A. 2018. Local protein solvation drives direct down-conversion in phycobiliprotein PC645 via incoherent vibronic transport. *Proc. Natl. Acad. Sci. U.S.A.* 115:E3342–E3350
 27. Cunningham K, Brand WC, Williams DF, Orlandi G. 1973. Vibronic intensity borrowing. Deuterium effect and emission—absorption asymmetry of the S1-S0 transition in pyrene. *Chem. Phys. Lett.* 20:496 – 500
 28. Avila Ferrer FJ, Improta R, Santoro F, Barone V. 2011. Computing the inhomogeneous broadening of electronic transitions in solution: a first-principle quantum mechanical approach. *Phys. Chem. Chem. Phys.* 13:17007–17012
 29. Nebgen B, Emmert FL, Slipchenko LV. 2012. Vibronic coupling in asymmetric bichromophores: theory and application to diphenylmethane. *J. Chem. Phys.* 137:084112
 30. Cerezo J, Avila Ferrer FJ, Prampolini G, Santoro F. 2015. Modeling solvent broadening on the vibronic spectra of a series of coumarin dyes. From implicit to explicit solvent models. *J. Chem. Theory Comput.* 11:5810–5825
 31. Santoro F, Jaquemin D. 2016. Going beyond the vertical approximation with time-dependent density functional theory. *Wiley Interdiscip. Rev.: Comput. Mol. Sci.* 6:460–486
 32. Zakaraya MG, Maisuradze GG, Ulstrup J. 1989. Theory of inhomogeneous environmental Gaussian broadening of resonance Raman excitation profiles for polyatomic molecules in solution. *J Raman Spectrosc.* 20:359–365
 33. Avila Ferrer FJ, Cerezo J, Soto J, Improta R, Santoro F. 2014. First-principle computation of absorption and fluorescence spectra in solution accounting for vibronic structure, temperature effects and solvent inhomogeneous broadening. *J. Chem. Theory Comput.* 1040-1041:328–337
 34. Halpin A, Johnson PJ, Tempelaar R, Murphy RS, Knoester J, et al. 2014. Two-dimensional spectroscopy of a molecular dimer unveils the effects of vibronic coupling on exciton coherences. *Nat. Chem.* 6:196–201
 35. Schlau-Cohen GS. 2015. Principles of light harvesting from single photosynthetic complexes. *Interface Focus* 5:20140088
 36. Dean JC, Scholes GD. 2017. Coherence spectroscopy in the condensed phase: insights into molecular structure, environment, and interactions. *Acc. Chem. Res.* 50:2746–2755
 37. Zuehlsdorff TJ, Montoya-Castillo A, Napoli JA, Markland TE, Isborn CM. 2019. Optical spectra in the condensed phase: capturing anharmonic and vibronic features using dynamic and static approaches. *J. Chem. Phys.* 151:074111
 38. Zuehlsdorff TJ, Isborn CM. 2019. Modeling absorption spectra of molecules in solution. *Int. J. Quantum Chem.* 119:e25719
 39. Roberts ST, Loparo JJ, Tokmakoff A. 2006. Characterization of spectral diffusion from two-dimensional line shapes. *J. Chem. Phys.* 125:084502
 40. Cho M. 2008. Coherent two-dimensional optical spectroscopy. *Chem. Rev.* 108:1331–1418
 41. Calhoun TR, Ginsberg NS, Schlau-Cohen GS, Cheng YC, Ballottari M, et al. 2009. Quantum coherence enabled determination of the energy landscape in light-harvesting complex II. *J. Phys. Chem. B* 113:16291–16295
 42. Rancova O, Abramavičius D. 2014. Static and dynamic disorder in bacterial light-harvesting complex LH2: a 2DES simulation study. *J. Phys. Chem. B* 118:7533–7540
 43. Dean JC, Rafiq S, Oblinsky DG, Cassette E, Jumper CC, Scholes GD. 2015. Broadband

- Transient Absorption and Two-Dimensional Electronic Spectroscopy of Methylene Blue. *J. Phys. Chem. A* 119:9098–9108
44. Fuller FD, Ogilvie JP. 2015. Experimental implementations of two-dimensional Fourier transform electronic spectroscopy. *Annu. Rev. Phys. Chem.* 66:667–690
 45. Dean JC, Oblinsky DG, Rafiq S, Scholes GD. 2016. Methylene blue exciton states steer nonradiative relaxation: ultrafast spectroscopy of methylene blue dimer. *J. Phys. Chem. B* 120:440–454
 46. Lee Y, Das S, Malamakal RM, Meloni S, Chenoweth DM, Anna JM. 2017. Ultrafast solvation dynamics and vibrational coherences of halogenated boron-dipyrromethene derivatives revealed through two-dimensional electronic spectroscopy. *J. Am. Chem. Soc.* 139:14733–14742
 47. Cipolloni M, Fresch B, Occhiuto I, Rukin P, Komarova KG, et al. 2017. Coherent electronic and nuclear dynamics in a rhodamine heterodimer-DNA supramolecular complex. *Phys. Chem. Chem. Phys.* 19:23043–23051
 48. Anda A, Abramavičius D, Hansen T. 2018. Two-dimensional electronic spectroscopy of anharmonic molecular potentials. *Phys. Chem. Chem. Phys.* 20:1642–1652
 49. Bolzonello L, Polo A, Volpato A, Meneghin E, Cordaro M, et al. 2018. Two-dimensional electronic spectroscopy reveals dynamics and mechanisms of solvent-driven inertial relaxation in polar BODIPY dyes. *J. Phys. Chem. Lett.* 9:1079–1085
 50. Maiuri M, Ostroumov EE, Sauer RG, Blankenship RE, Scholes GD. 2018. Coherent wavepackets in the Fenna–Matthews–Olson complex are robust to excitonic-structure perturbations caused by mutagenesis. *Nat. Chem.* 10:177–183
 51. Franck J. 1925. Elementary processes of photochemical reactions. *J. Trans. Faraday Soc.* 21:536–542
 52. Condon E. 1926. A Theory of intensity distribution in band systems. *Phys. Rev.* 28:1182–1201
 53. Cederbaum LS, Domcke W. 1976. A many-body approach to the vibrational structure in molecular electronic spectra. I. Theory. *J. Chem. Phys.* 64:603
 54. Roche M. 1990. On the polyatomic Franck-Condon factors. *Chem. Phys. Lett.* 168:556–558
 55. Islampour R, Dehestani M, Lin SH. 1999. A new expression for multidimensional Franck-Condon integrals. *J. Mol. Spectrosc.* 194:179–184
 56. Toniolno A, Persico M. 1999. Efficient calculation of Franck-Condon factors and vibronic couplings in polyatomics. *J. Comput. Chem.* 22:968–975
 57. Luis JM, Torrent-Sucarrat M, Solà M. 2005. Calculation of Franck-Condon factors including anharmonicity: simulation of the $C_2H_4^+ X^2B_{3u} \leftarrow C_2H_4 X^1A_g$ band in the photoelectron spectrum of ethylene. *J. Chem. Phys.* 122:184104
 58. Small GJ. 1971. Herzberg-Teller vibronic coupling and the Duschinsky effect. *J. Chem. Phys.* 54:3300–3306
 59. Santoro F, Barone V. 2009. Computational approach to the study of the lineshape of absorption and electronic circular dichroism spectra. *J. Quantum Chem.* 110:476–486
 60. Niu Y, Peng Q, Deng C, Gao X, Shuai Z. 2010. Theory of excited state decays and optical spectra: application to polyatomic molecules. *J. Phys. Chem. A* 114:7817–7831
 61. Avila Ferrer FJ, Barone V, Cappelli C, Santoro F. 2013. Duschinsky, Herzberg–Teller, and multiple electronic resonance interferential effects in resonance Raman spectra and excitation profiles. *J. Chem. Theory Comput.* 9:3597–3611
 62. Mukazhanova A, Trerayapiwat KJ, Mazaheripour A, Wardrip AG, Frey NC, et al. 2020. Accurate first-principles calculation of the vibronic spectrum of stacked perylene tetracarboxylic acid diimides. *J. Phys. Chem. A* 124:3055–3063
 63. Li SL, Truhlar DG. 2017. Franck-Condon models for simulating the band shape of electronic absorption spectra. *J. Chem. Theory Comput.* 13:2823–2830
 64. de Souza B, Neese F, Izsák R. 2018. On the theoretical prediction of fluorescence rates from first principles using the path integral approach. *J. Chem. Phys.* 148:034104
 65. Miertuš S, Scrocco E, Tomasi J. 1981. Electrostatic interaction of a solute with a continuum.

- A direct utilization of ab initio molecular potentials for the prediction of solvent effects. *Chem. Phys.* 55:117–129
66. Cammi R, Tomasi J. 1995. Remarks on the use of the apparent surface charges (ASC) methods in solvation problems: iterative versus matrix-inversion procedures and the renormalization of the apparent charges. *J. Comput. Chem* 16:1449–1458
 67. Cossi M, Scalmani G, Rega N, Barone V. 2002. New developments in the polarizable continuum model for quantum mechanical and classical calculations on molecules in solution. *J. Chem. Phys.* 117:43–54
 68. Scalmani G, Frisch MJ. 2010. Continuous surface charge polarizable continuum models of solvation. I. General formalism. *J. Chem. Phys.* 132
 69. Mennucci B. 2012. Polarizable continuum model. *Wiley Interdiscip. Rev. Comput. Mol. Sci.* 2:386–404
 70. Roux B, Simonson T. 1999. Implicit solvent models. *Biophys. Chem.* 78:1 – 20
 71. Cramer CJ, Truhlar DG. 1999. Implicit solvation models: equilibria, structure, spectra, and dynamics. *Chem. Rev.* 99:2161–2200
 72. Coon J, DeWames R, Loyd C. 1962. The Franck-Condon principle and the structures of excited electronic states of molecules. *J. Mol. Spectrosc.* 8:285 – 299
 73. Malcioglu OB, Calzolari A, Gebauer R, Varsano D, Baroni S. 2011. Dielectric and thermal effects on the optical properties of natural dyes: a case study on solvated cyanin. *J. Am. Chem. Soc.* 133:15425–15433
 74. Retegan M, Neese F, Pantazis DA. 2013. Convergence of QM/MM and cluster models for the spectroscopic properties of the oxygen-evolving complex in photosystem II. *J. Chem. Theory Comput.* 9:3832–3842
 75. De Mitri N, Monti S, Prampolini G, Barone V. 2013. Absorption and emission spectra of a flexible dye in solution: a computational time-dependent approach. *J. Chem. Theory Comput.* 9:4507–4516
 76. Valsson O, Campomanes P, Tavernelli I, Rothlisberger U, Filippi C. 2013. Rhodopsin absorption from first principles: bypassing common pitfalls. *J. Chem. Theory Comput.* 9:2441–2454
 77. Provorse MR, Peev T, Xiong C, Isborn CM. 2016. Convergence of excitation energies in mixed quantum and classical solvent: comparison of continuum and point charge models. *J. Phys. Chem. B* 120:12148–12159
 78. Zuehlsdorff TJ, Haynes PD, Hanke F, Payne MC, Hine NDM. 2016. Solvent effects on electronic excitations of an organic chromophore. *J. Chem. Theory Comput.* 12:1853–1861
 79. Tapavicza E, Furche F, Sundholm D. 2016. Importance of vibronic effects in the UV-Vis spectrum of the 7,7,8,8-tetracyanoquinodimethane anion. *J. Chem. Theory Comput.* 12:5058–5066
 80. Zuehlsdorff TJ, Haynes PD, Payne MC, Hine NDM. 2017. Predicting solvatochromic shifts and colours of a solvated organic dye: the example of Nile red. *J. Chem. Phys.* 146:124504
 81. Milanese JM, Provorse MR, Alameda E, Isborn CM. 2017. Convergence of computed aqueous absorption spectra with explicit quantum mechanical solvent. *J. Chem. Theory Comput.* 13:2159–2171
 82. Walker RC, Crowley MF, Case DA. 2007. The implementation of a fast and accurate QM/MM potential method in Amber. *J. Comput. Chem.* 29:1019–1031
 83. Senthilkumar K, Mujika JI, Ranaghan KE, Manby FR, Mulholland AJ, Harvey JN. 2008. Analysis of polarization in QM/MM modelling of biologically relevant hydrogen bonds. *J. Royal Soc. Interface* 5:S207–S216
 84. Beierlein FR, Michel J, Essex JW. 2011. A simple QM/MM approach for capturing polarization effects in protein-ligand binding free energy calculations. *J. Phys. Chem. B* 115:4911–4926
 85. Jurinovich S, Viani L, Prandi IG, Renger T, Mennucci B. 2015. Towards an ab initio description of the optical spectra of light-harvesting antennae: application to the CP29 complex of photosystem II. *Phys. Chem. Chem. Phys.* 17:14405–14416

86. Kulik HJ, Zhang J, Klinman JP, Martinez TJ. 2016. How large Should the QM region be in QM/MM calculations? The case of catechol *O*-methyltransferase. *J. Phys. Chem. B* 120:11381–11394
87. Karelina M, Kulik HJ. 2017. Systematic quantum mechanical region determination in QM/MM simulation. *J. Chem. Theory Comput.* 13:563–576
88. Loco D, Jurinovich S, Cupellini L, Menger MFSJ, Mennucci B. 2018. The modeling of the absorption lineshape for embedded molecules through a polarizable QM/MM approach. *Photochem. Photobiol. Sci.* 17:552–560
89. Zuehlsdorff TJ, Napoli JA, Milanese JM, Markland TE, Isborn CM. 2018. Unraveling electronic absorption spectra using nuclear quantum effects: photoactive yellow protein and green fluorescent protein chromophores in water. *J. Chem. Phys.* 149:024107
90. Zuehlsdorff TJ, Isborn CM. 2018. Combining the ensemble and Franck-Condon approaches for calculating spectral shapes of molecules in solution. *J. Chem. Phys.* 148:024110
91. Shedge SV, Zuehlsdorff TJ, Servis MJ, Clark AE, Isborn CM. 2019. Effect of ions on the optical absorption spectra of aqueously solvated chromophores. *J. Phys. Chem. A* 123:6175–6184
92. Zuehlsdorff TJ, Hong H, Shi L, Isborn CM. 2020. Influence of electronic polarization on the spectral density. *J. Phys. Chem. B* 124:531–543
93. Horton JT, Allen AEA, Dodda LS, Cole DJ. 2019. QUBEKit: automating the derivation of force field parameters from quantum mechanics. *J. Chem. Inf. Model* 59:1366–1381
94. Behler J, Parrinello M. 2007. Generalized neural-network representation of high-dimensional potential-energy surfaces. *Phys. Rev. Lett.* 98:1–4
95. Bartók AP, Payne MC, Kondor R, Csányi G. 2010. Gaussian approximation potentials: the accuracy of quantum mechanics, without the electrons. *Phys. Rev. Lett.* 104:1–4
96. Wang LP, Martinez TJ, Pande VS. 2014. Building force fields: an automatic, systematic, and reproducible approach. *J. Phys. Chem. Lett.* 5:1885–1891
97. Khorshidi A, Peterson AA. 2016. Amp: a modular approach to machine learning in atomistic simulations. *Comput. Phys. Commun.* 207:310–324
98. Artrith N, Urban A. 2016. An implementation of artificial neural-network potentials for atomistic materials simulations: performance for TiO₂. *Comput. Mater. Sci.* 114:135–150
99. Wang LP, McKiernan KA, Gomes J, Beauchamp KA, Head-Gordon T, et al. 2017. Building a more predictive protein force field: a systematic and reproducible route to AMBER-FB15. *J. Phys. Chem. B* 121:4023–4039
100. Chen MS, Zuehlsdorff TJ, Morawietz T, Isborn CM, Markland TE. 2020. Exploiting machine learning to efficiently predict multidimensional optical spectra in complex environments. *J. Phys. Chem. Lett.* 11:7559–7568
101. Marx D, Parrinello M. 1996. Ab initio path integral molecular dynamics: basic ideas. *J. Chem. Phys.* 104:4077–4082
102. Svoboda O, Ončák M, Slavíček P. 2011. Simulations of light induced processes in water based on ab initio path integrals molecular dynamics. II. Photoionization. *J. Chem. Phys.* 135:154302
103. Ceriotti M, Parrinello M, Markland TE, Manolopoulos DE. 2010. Efficient stochastic thermostatting of path integral molecular dynamics. *J. Chem. Phys.* 133:124104
104. Markland TE, Ceriotti M. 2018. Nuclear quantum effects enter the mainstream. *Nat. Rev. Chem.* 2:1–14
105. Tuckerman ME, Ungar PJ, Von Rosenvinge T, Klein ML. 1996. Ab initio molecular dynamics simulations. *J. Phys. Chem.* 100:12878–12887
106. Tozzini V, Nifosì R. 2001. Ab initio molecular dynamics of the green fluorescent protein (GFP) chromophore: an insight into the photoinduced dynamics of green fluorescent proteins. *J. Phys. Chem. B* 105:5797–5803
107. Ko C, Levine B, Toniolo A, Manohar L, Olsen S, et al. 2003. Ab initio excited-state dynamics of the photoactive yellow protein chromophore. *J. Am. Chem. Soc.* 125:12710–12711
108. Weingart O, Schapiro I, Buss V. 2007. Photochemistry of visual pigment chromophore models

- by ab initio molecular dynamics. *J. Phys. Chem. B* 111:3782–3788
109. Zwier MC, Shorb JM, Krueger BP. 2007. Hybrid molecular dynamics-quantum mechanics simulations of solute spectral properties in the condensed phase: evaluation of simulation parameters. *J. Comput. Chem.* 28:1572–1581
 110. Rosnik AM, Curutchet C. 2015. Theoretical characterization of the spectral density of the water-soluble chlorophyll-binding protein from combined quantum mechanics/molecular mechanics molecular dynamics simulations. *J. Chem. Theory Comput.* 11:5826–5837
 111. Chandrasekaran S, Aghtar M, Valleau S, Aspuru-Guzik A, Kleinekathöfer U. 2015. Influence of force fields and quantum chemistry approach on spectral densities of BChl_a in solution and in FMO proteins. *J. Phys. Chem. B* 119:9995–10004
 112. Kim CW, Park JW, Rhee YM. 2015. Effect of chromophore potential model on the description of exciton–phonon interactions. *J. Phys. Chem. Lett.* 6:2875–2880
 113. Lee MK, Coker DF. 2016. Modeling electronic-nuclear interactions for excitation energy transfer processes in light-harvesting complexes. *J. Phys. Chem. Lett.* 7:3171–3178
 114. Andreussi O, Prandi IG, Canpetella M, Prampolini G, Mennucci B. 2017. Classical force fields tailored for QM applications: is it really a feasible strategy? *J. Chem. Theory Comput.* 13:4636–4648
 115. Ferrer FJA, Davari MD, Morozov D, Groenhof G, Santoro F. 2014. The lineshape of the electronic spectrum of the green fluorescent protein chromophore, part II: solution phase. *ChemPhysChem* 15:3246–3257
 116. Zalesny R, Murugan NA, Gel'mukhanov F, Rinkevicius Z, Ośmiałowski B, et al. 2015. Toward fully nonempirical simulations of optical band shapes of molecules in solution: a case study of heterocyclic ketoimine difluoroborates. *J. Phys. Chem. A* 119:5145–5152
 117. Loco D, Cupellini L. 2018. Modeling the absorption lineshape of embedded systems from molecular dynamics: A tutorial review. *Int. J. Quantum Chem.* 119:e25726
 118. Cerezo J, Aranda D, Avila Ferrer FJ, Prampolini G, Santoro F. 2020. Adiabatic-molecular dynamics generalized vertical Hessian approach: a mixed quantum classical method to compute electronic spectra of flexible molecules in the condensed phase. *J. Chem. Theory Comput.* 16:1215–1231
 119. Del Galdo S, Fusè M, Barone V. 2020. The ONIOM/PMM model for effective yet accurate simulation of optical and chiroptical spectra in solution: camphorquinone in methanol as a case study. *J. Chem. Theory Comput.* 16:3294–3306
 120. Fortino M, Collini E, Pedone A, Bloino J. 2020. Role of specific solute–solvent interactions on the photophysical properties of distyryl substituted BODIPY derivatives. *Phys. Chem. Chem. Phys.* 22:10981–10994
 121. Mukamel S. 1995. *Principles of Nonlinear Optical Spectroscopy*. New York: Oxford University Press
 122. Mukamel S, Abramavicius D. 2004. Many-body approaches for simulating coherent nonlinear spectroscopies for electronic and vibrational excitons. *Chem. Rev.* 104:2073–2098
 123. Li B, Johnson AE, Mukamel S, Myers AB. 1994. The Brownian oscillator model for solvation effects in spontaneous light emission and their relationship to electron transfer. *J. Am. Chem. Soc.* 116:11039–11047
 124. Duschinsky F. 1937. On the interpretation of electronic spectra of polyatomic molecules. *Acta Physicochim. URSS* 7:551
 125. Bader JS, Berne BJ. 1994. Quantum and classical relaxation rates from classical simulations. *J. Chem. Phys.* 100:8359
 126. Egorov SA, Everitt KF, Skinner JL. 1999. Quantum dynamics and vibrational relaxation. *J. Phys. Chem. A* 103:9494–9499
 127. Kim H, Rossky PJ. 2002. Evaluation of quantum correlation functions from classical data. *J. Phys. Chem. B* 106:8240
 128. Jung KA, Videla PE, Batista VS. 2018. Inclusion of nuclear quantum effects for simulations

- of nonlinear spectroscopy. *J. Chem. Phys.* 148:244105
129. Anda A, De Vico L, Hansen T, Abramavičius. 2016. Absorption and fluorescence lineshape theory for polynomial potentials. *J. Chem. Theory Comput.* 12:5979–5989
 130. Avila Ferrer FJ, Santoro F. 2012. Comparison of vertical and adiabatic harmonic approaches for the calculation of the vibrational structure of electronic spectra. *Phys. Chem. Chem. Phys.* 14:13549–13563
 131. Davis MM, Helzer HB. 1966. Titrimetric and equilibrium studies using indicators related to Nile blue A. *Anal. Chem.* 38:451–461
 132. Yanai T, Tew DP, Handy NC. 2004. A new hybrid exchange-correlation functional using the Coulomb-attenuating method (CAM-B3LYP). *Chem. Phys. Lett.* 393:51–57
 133. Kubo R. 1963. The fluctuation-dissipation theorem. *Rep. Prog. Phys.* 59:1665–1735
 134. Craig IR, Manolopoulos DE. 2004. Quantum statistics and classical mechanics: real time correlation functions from ring polymer molecular dynamics. *J. Chem. Phys.* 121:3368
 135. Ramirez R, Lopez-Ciudad T, P PK, Marx D. 2004. Quantum corrections to classical time-correlation functions: hydrogen bonding and anharmonic floppy modes. *J. Chem. Phys.* 121:3973
 136. Valleau S, Eisfeld A, Aspuru-Guzik A. 2012. On the alternatives for bath correlators and spectral densities from mixed quantum-classical simulations. *J. Chem. Phys.* 137:224103
 137. Zuehlsdorff TJ, Hong H, Shi L, Isborn CM. 2020. Nonlinear spectroscopy in the condensed phase: the role of duschinsky rotations and third order cumulant contributions. *J. Chem. Phys.* 153:044127
 138. Zuehlsdorff TJ, Hine NDM, Spencer JS, Harrison NM, Riley DJ, Haynes PD. 2013. Linear-scaling time-dependent density-functional theory in the linear response formalism. *J. Chem. Phys.* 139:064104
 139. Zuehlsdorff TJ, Hine NDM, Payne MC, Haynes PD. 2015. Linear-scaling time-dependent density-functional theory beyond the Tamm-Dancoff approximation: obtaining efficiency and accuracy with in situ optimised local orbitals. *J. Chem. Phys.* 143:204107
 140. Seritan S, Bannwarth C, Fales BS, Hohenstein EG, Isborn CM, et al. 2020. Terachem: a graphical processing unit-accelerated electronic structure package for large-scale ab initio molecular dynamics. *WIREs Comput. Mol. Sci.* :e1494

REFERENCE ANNOTATIONS

12. Bondanza. A recent review that provides a good overview of polarizable embedding QM/MM and its application to spectroscopy and dynamics simulations.
22. Baiardi. Showcases time-dependent approach for Franck-Condon calculations. Ref [64], de Souza et al, presents the more mathematically stable formulation.
117. Loco. A tutorial review that provides a good starting point for spectroscopy calculations within the dynamic approach.
118. Cerezo / Santoro. Here Santoro and co-workers apply the sumFC method within a vertical Hessian approach for additional computational savings.
121. Mukamel. A fundamental book detailing many aspects of nonlinear spectroscopy. A more approachable set of notes can be found online by Peter Hamm, “Principles of Nonlinear Optical Spectroscopy: A Practical Approach.”